VIDWAN Journal of Science, Technology and Innovation

OPEN ACCESS

PEER-REVIEWED - OPEN ACCESS Vol. 01 · Issue 01 · 2026 · pp. 38- 49 | ISSN: APPLIED (Online) | INAGURAL EDITION

Spin-Orbit Torque-Driven Field-Free Switching Of Perpendicular Magnetization In Ferromagnetic Layers With Vertical Composition Gradients

Dr.D.N.V. Krishna Reddy, *Department of Management Studies,*
Sai Spurthy Institute of Technological Sciences , Sathupally, TG.

ABSTRACT

The current-induced spin-orbit torques (SOTs) are fascinating because they allow the magnetic order in spintronic devices to be changed quickly and efficiently. However, a way to disrupt the symmetry in the material's plane is needed to guarantee that the transition of perpendicularly magnetic materials through SOT can be anticipate. Modern approaches to this problem include increasing the device's in-plane bias magnetic field strength or altering its design to be less uniform throughout the device's axis of rotation. Both of these plans, however, might be difficult to implement. In this case, we show how SOT switching works in a single, straight CoTb layer with a vertical composition gradient built without the bias element. During the switching phase, the in-plane symmetry is disrupted by a gradient-driven Dzyaloshinskii-Moriya interaction (g-DMI) and substantial intrinsic SOTs caused by the vertical structural inversion asymmetry. Experimental results are confirmed by micromagnetic models that explain the connection between g-DMI and deterministic switching to carry out. Using the bias-field-free switching strategy, g-DMI allows us to fabricate small, functional SOT devices for perpendicular ferrimagnets.

Keywords: *Orbit; Torque; Magnetization; Ferromagnetic; gradient-driven Dzyaloshinskii-Moriya interaction (g-DMI)*

Article history: Received 10 July 2026 · Revised 20 July 2026 · Accepted 28 July 2026 · Published 9 July 2026

1. INTRODUCTION

It seems that spin-orbit torque (SOT) is a fast and low-power way to adjust the magnetic order in spintronic devices. Applications requiring fast on-chip memory, such as high-performance computing and artificial intelligence, are prime examples of this. There is a lot of interest right now in ferrimagnetic (FIM) material SOT switching. The exchange-dominated nature of the high-frequency (sub-terahertz) antiferromagnet dynamics is observed in FIMs. Fast switching rates are possible, in contrast to antiferromagnets that have problems controlling their domain sizes. Also, because they aren't magnetically zero, they can use the simple electrical feedback methods that work with ferromagnetic material systems.

As a result, FIMs may soon be able to serve as realistic, high-performing SOT devices. Memory devices that use magnets with perpendicular magnetic anisotropy (PMA) often implement SOT switching in a non-magnet/ferromagnet (NM/FM) or NM/FIM heterostructure. To do this, we need an external in-plane magnetic field, denoted as Hex, which runs parallel to the direction of the current. When the Rashba effect1 happens at the NM/FM interface or when the spin Hall effect (SHE) happens in the NM, the adjacent magnetization might transition (for example, in topological insulators or heavy metals). But Hex disrupts the symmetry of in-plane inversion, therefore for any given in-plane current direction, the direction of switching is predictable.

However, due to the need for external Hex in switching, incorporating SOT devices within semiconductor circuits becomes more challenging. Researchers are looking for structural or magnetic ways to break the in-plane symmetry that Hex provides so that they can build practical SOT memory devices. For instance, up until now, it has been difficult to combine many spin torque sources into a single device due to factors such as in-plane structure, compositional or interfacial oxidation asymmetry, plane exchange bias fields, and interlayer exchange coupling. Some methods that use several torque sources are distinct from others, though, and this is due to the fact that they depend on breaking the device's static in-plane symmetry. This is a common problem when making large groups of devices with the same specifications on the same silicon wafer. Instead, we show experimentally that predictable switching may be achieved by structures with plane symmetry and growth direction asymmetry. This is because, during the switching phase, the Dzyaloshinskii-Moriya interaction (DMI) causes a dynamical break in the plane of symmetry. With the help of the DMI effect, one can make spin images that have broken chiral symmetry. Domain barriers and skyrmions could be what these are.

Hence, DMI has been suggested as a way to break symmetry and enable deterministic switching without an external field when coupled with SOTs that act as damping devices and fields. The combined operation of DMI and SOT has not yet established a scenario of field-free predictable switching. Prior research that found a big bulk DMI in a rare-earth (RE)-transition-metal (TM) ferrimagnet (FIM) motivated us to create the necessary DMI. Because dense metals naturally have an uneven distribution of components, a vertical com position gradient was present in this case. We achieve a vertical composition difference in the FIM layer by adding very thin layers with different RE/TM ratios. This improves the DMI's performance. Consequently, the inversion symmetry is broken by the growth path.

The majority of FIM use a gradient-driven DMI (g-DMI) because of the constant composition gradient. But just like the interfacial DMI in NM/FIM and NM/FM systems that was discussed earlier, it keeps the same symmetry. Plus, because of their strong spin-orbit coupling (SOC), RE elements can generate spin currents that are similar to those of nonmagnetic 5d metals like Pt, which are on the other end of the 5d metal spectrum. This is mostly due to their 5D band. The f electrons of Tb are not involved in the transmission process. Having said that, the SOC of the 3d electrons in cobalt is much lower.

When high spin-orbit coupling and broken inversion symmetry come together, it leads to Rashba interactions. These interactions lead to spin currents and Rashba spin polarizations caused by currents. The possibility of these spin currents inducing a SOT on the FIM magnetization will be addressed in the section that follows. We show that one ferromagnetic CoTb layer with a vertical composition gradient can efficiently perform field-free SOT magnetization switching by combining g-DMI and SOT. This can concurrently remove the need for both NM and Hex in the SOT switching devices stated above, as shown in experiments and models. Micromagnetic models are supported by the results of field-free switching. Our work opens the possibility of field-free on/off control of perpendicular ferrimagnets. This might be accomplished using large, homogeneous wafers.

2. RESULTS

Changes in Tb composition lead to the noticeable SOT. As a ferrimagnetic alloy with strong PMA in a wide range of ratios, CoTb is made possible by the non-magnetic link between its R and T components. The exact range of PMA's constituents was determined by applying a series of Al (2 nm)/Co1-aTba (6 nm)/Al (3 nm) coatings to heated and oxidized silicon surfaces (see Fig. 1a). The amount of lead in the metal was shown by A. In this case, Al was chosen because to its exceptionally low SOT. To change the stoichiometry of the final CoTb layer, Co and Tb were sputtered together at different intensities. as shown in the illustration. Among them are 1b, Co0.56Tb0, and Co0.87Tb0.13.

The samples' elevated Tb and Co concentrations helped the heterostructure exhibit desirable PMA properties. Fitting the composition to the net saturation magnetization Ms also allowed for the discovery of Co0.71Tb0. was found to be the room-temperature magnetic equilibrium point. Following the provision of this information, samples exhibiting a variance in vertical composition were deposited. similar to the one in Figure. Eleven layers of CoTb, with a thickness of one nanometer apiece, compose the ferrimagnet in 1c. The lowest layer's composition stayed at Co0.87Tb0.13. Consequently, the difference was μ per nanometer.

A specific stage in the composition of Tb was followed by the last five layers that were deposited. The formula for their composition, for n = 1, 2, 3, 4, and 5, is Co0.87-nμTb0.13+nμ. According to Figure 1d, the sample's total Ms falls as the composition gradient rises, which agrees with the trend of the Co-rich portion in Figure. The sample gets closer to the magnetic adjustment point8,9 as the average Tb content increases, as seen in 1b. When $\varepsilon = 0.07$, the sample is almost balanced, with $M_s < 50$ emu/cc. However, when $\varepsilon = 0.08$ or higher, the sample starts to show an in-plane magnetic component. So, we do not cover any slopes μ outside of the range of 0 to 0.07.

We used energy-dispersive X-ray spectroscopy (EDS) and high-resolution cross-sectional scanning transmission electron microscopy (STEM) on the sample with $\varepsilon = 0.07$ to confirm the presence of the composition gradient and find its magnitude. Figure 1e presents a logical representation of the sample's layer arrangement. It was expected that the CoTb layer would be amorphous due to its lack of a clear crystal structure. To the right of the thickness direction is shown the relationship between the EDS types. It is clear from 1f that the Co and Tb components are not evenly distributed.

The location where the probe was found to have pierced the substrate is in agreement with the planned structure shown in Figure. because Co (Tb) intensity is going up (down). 1c. So that electrical testing could be conducted on them, the films were transformed into 10 µm thick Hall bar devices using ion milling and conventional lithography. the inside of the graphic. Figure 2a depicts the setup of the device and the connections for measurements. The results of the film-level magnetometry are in agreement with the anomalous Hall effect resistance (RAHE) measurements, which indicate that each sample has a distinct PMA. Figure. This is a picture of what could happen if ε equals 0.06. Part 2a. Analyze the RAHE loop's orientation maintenance behavior as δ changes from 0.00 to 0.07. This suggests that the bulk of samples still consist of Corich.

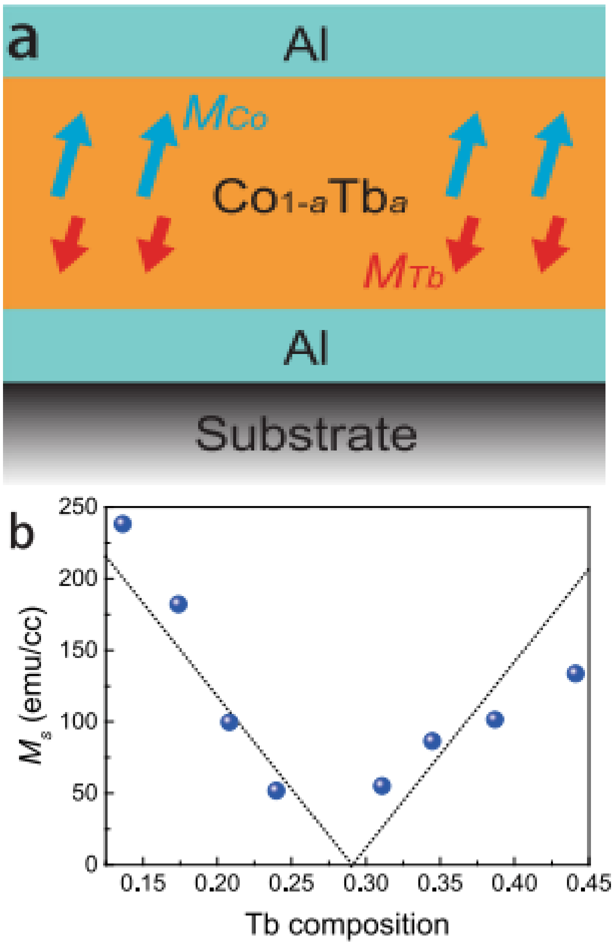

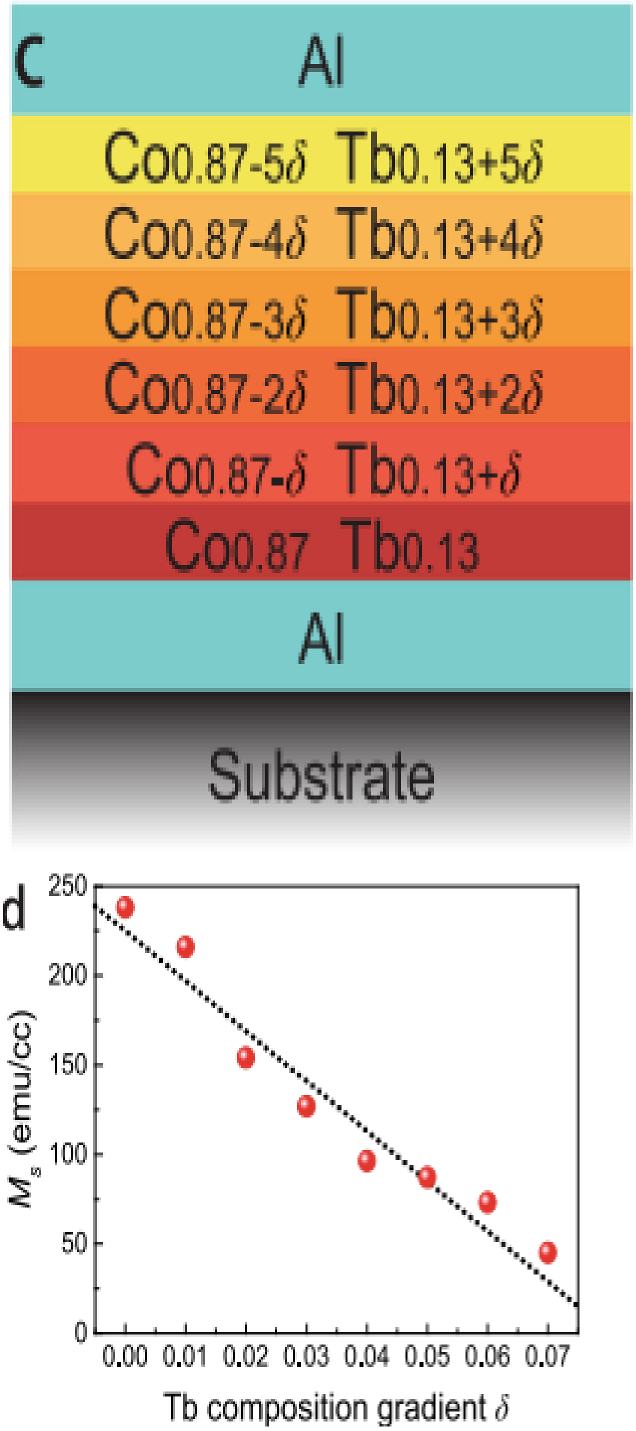
c
Al
Co0.87-5δ Tb0.13+5δ
Co0.87-4δ Tb0.13+4δ
Co0.87-3δ Tb0.13+3δ
Co0.87-2δ Tb0.13+2δ
Co0.87-δ Tb0.13+δ
Co0.87 Tb0.13
Al
Substrate
d
Ms (emu/cc)
250
200
150
100
50
0
0.00 0.01 0.02 0.03 0.04 0.05 0.06 0.07
Tb composition gradient δ

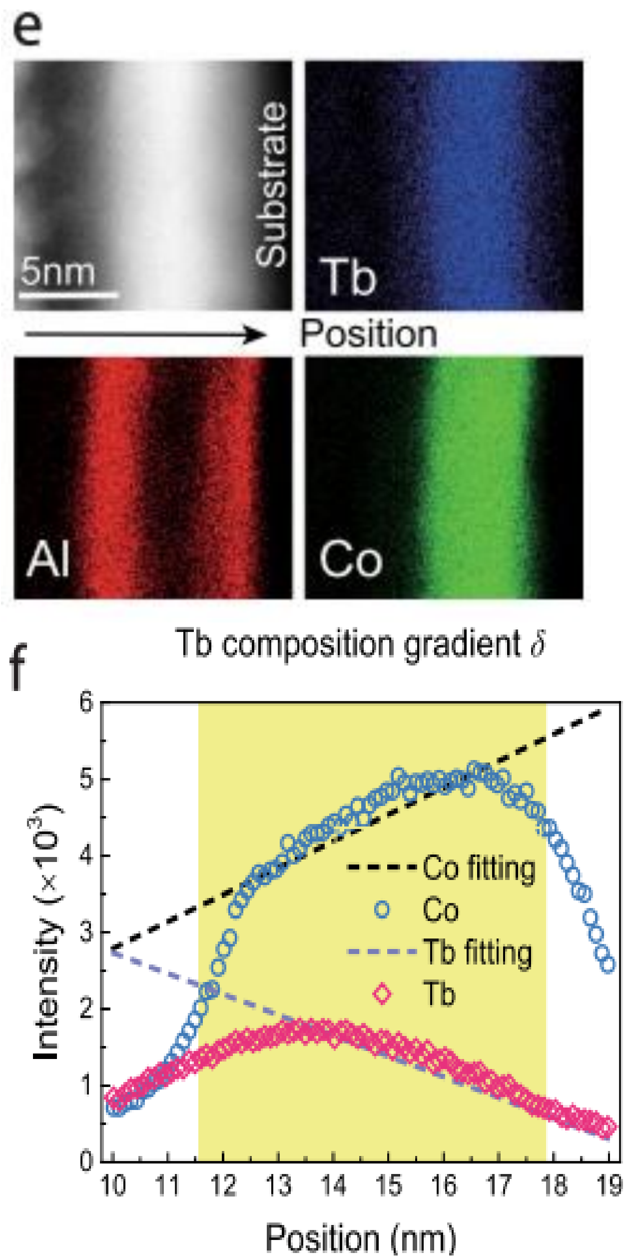

Figure. 1. An alternating composition gradient on CoTb sheets: structure and characterisation. Every one of the Co1-aTba instances follows the same blueprint. b The net magnetization of similar CoTb samples is dependent on the concentration of Tb. At a Tb concentration of 0.29, a magnetization compensation point becomes apparent. The structure of the c CoTb sample exhibits compositional variation denoted as ε. As ε grows, the net magnetization falls in a linear fashion. ε-values of 0.07 indicate that STEM images of the sample are accessible. The amount of Co and Tb present was found to be altered by the vertical placement of the sample, according to EDS. Contrary gradients in the amounts of Co and Tb prove that the composition gradient is correct and going in the correct way.

Next, we used standard harmonic tests across a wide field range to find each sample's effective spin Hall angle and SOT efficiency. So long as there is a countercurrent

At the equilibrium point, when the x-axis alternating effective field created by SOT is applied, magnetization oscillations will occur. The second-harmonic Hall resistance R2ܼ rises as a result. When compared to the magnetic field on a plane, the distorted one is less powerful.

By applying the equation, the field Hk, R2ω can be determined.

$$R_{2\omega} = \frac{1}{2}\frac{R_{AHE}H_{DL}}{|H_x| - H_k} + R_{offset}, \qquad (1)$$

where HDL stands for resistance offset and Roffset for damping-like SOT effective field. The sample's first harmonic resistances, Rϋ and R2ϋ, are shown in Figures 2b and c. The value of ε comes to 0.06. Modifying Fig. Use the equation to find 2c. The SOT efficiency, denoted as ξ, is 3.2 ± 0.3 Oe/(1010 A/m2), where jCoTb is the current density in the CoTb layer. Supplementary Note S1 presents the jCoTb computation.

The damping-like effective spin Hall angle was then calculated using the formula θDL = 2eMstCoTbHDL/ℏjCoTb, where tCoTb is the thickness of the CoTb layer. Figure. proceeds to combine the DL values of samples that have different slopes. After that. It's interesting to observe that DL seems to grow together with ε. The effective spin Hall angle shown in Pt10 is nearly identical to the maximum value of θDL for ε = 0.07, which is 0.061 ± 0.006.

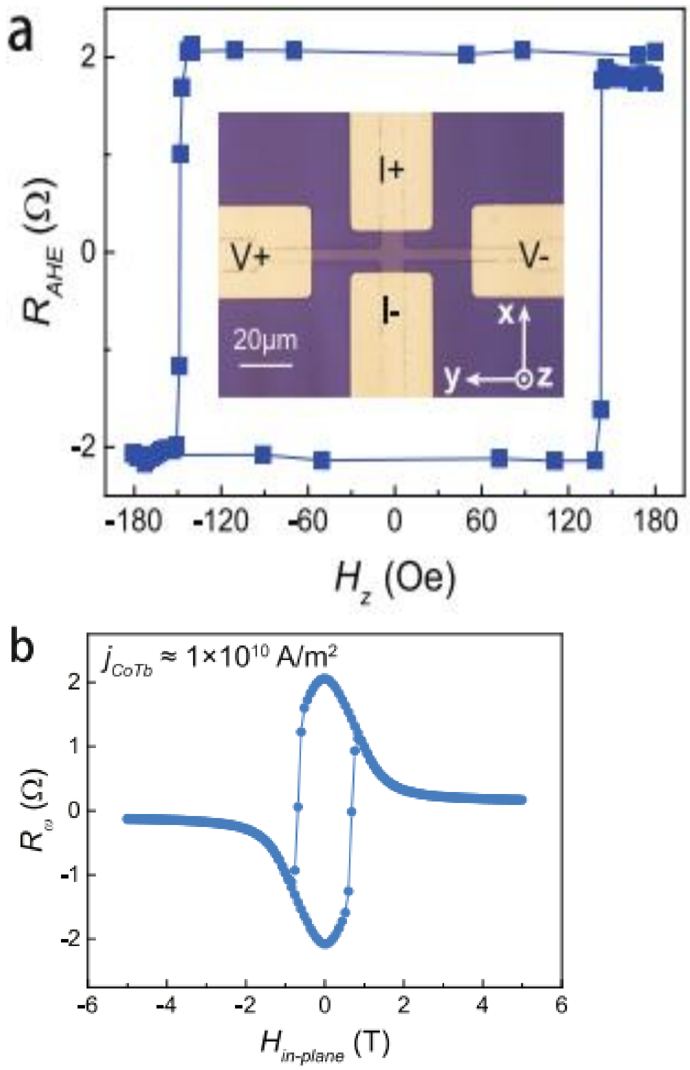

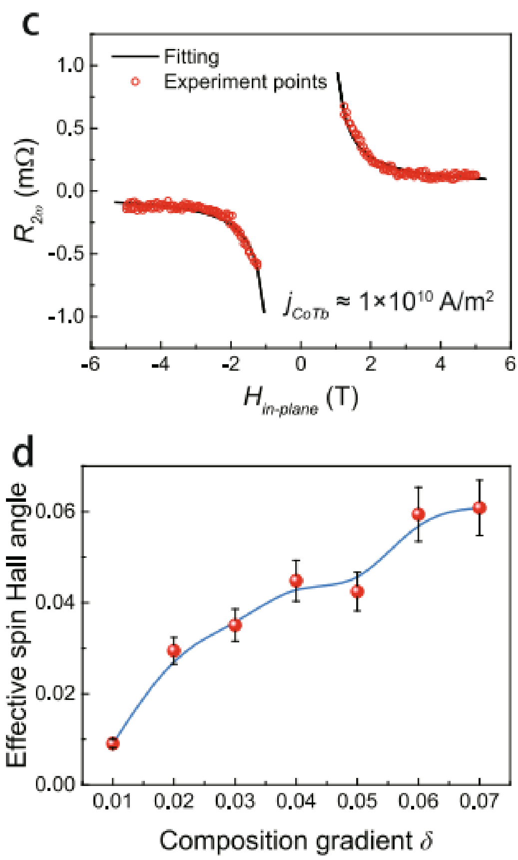

Figure. 2. drawing up an electrical test and explaining a SOT. This sample with ε = 0.06 has had an AHE loop tested. Samples with perpendicular magnetization have a square form. Pictured in the inset is a standard Hall bar device. Rü against b = 0. the sample's magnetic field along the x-axis with ε = 0.06. The sample with δ = 0.06 and jCoTb = 1 × 10^5 A/m2 is shown in Figures C R2ü and the fitted line vs. magnetic field along the x-axis. We should expect DL's strength to increase in tandem with the cosmetics gradient. The error bars for each sample are determined by obtaining R2ü values at different current densities.

This large SOT is found because of the broken inversion symmetry and strong spin-orbit coupling in our structure, which cause current-induced Rashba spin polarizations and spin currents. Our observed composition gradients or non-symmetric interfaces can disrupt the inversion symmetry of a magnetic layer according to the traditional model of Manchon and Zhang. The name "g-Rashba" might be used for these, which is similar to the word "g-DMI" that was previously used for DMI. The spin currents generated by Rashba and the more general idea put out by Stiles and colleagues are detailed in Note S1. There are two kinds of symmetry in magnetic or ferrimagnetic materials. One is the spin anomalous hall effect (SAHE) symmetry, which occurs when the spin is aligned with the magnetization (M) axis. The other is the spin homology effect (SHE) symmetry, which occurs when the spin is aligned with the y axis, allowing emission down the z axis and current along the x axis.

The SAHE term loses its ability to attract magnetization M when it is polarized with M. In the presence of a potential for spin transport, whether inside the magnetic layer or between its various areas, the SHE-like spin current in a magnetic layer can generate a Damping-Like (DL) spin transfer force acting on M. Weak absorber Al and two thin layers of light element prevent the CoTb layer's magnetic from penetrating our samples' exteriors. Nevertheless, the unequal distribution of CoTb layers with various compositions—showing higher Rashba spin polarization and 5d concentrations at the top—could lead to spin transfers that don't exist in other parts of the sample. Our samples should exhibit a bottom-to-top magnetic orientation for the larger downhill spin currents, which are emitted from above, and an upward-to-top magnetic orientation for the smaller upward spin currents, which are emitted from below with opposite spin polarization. However, these movements shouldn't be identical. Finding the final torque is difficult since it is dependent on many parameters such as the gradient of Tb concentration, the variation of the Rashba interaction, and the spin dephasing length, which controls the amount of spin transfer. As the bracket shows an effective spin Hall angle ¸DL, which is zero when the layer is flat, the DL torque should nearly represent an order spin current.

Switching vertical CoTb utilizing gradient-driven DMI and SOT eliminates the need for a field. The CoTb samples that had a vertical composition gradient were further tested for magnetization switching using SOT. The figure shows how the measurement method is put into practice. A little detecting current of 0.1 mA (blue triangles) was applied after each writing current pulse in 3a. This current went through a positive, negative, and positive cycle (orange bars) in 0.1 ms. The status of the magnetism might then be better ascertained using RAHE. The relationship between the RAHE and the write current density jCoTb is seen in Figure 3b for the sample where ε = 0.07 and a bias field Hex that travels from 100 Oe to -100 Oe down the x-axis. The presence of intrinsic SOTs with a compositional gradient in the CoTb is indicated by the successful magnetization switch.

The current-driven RAHE, on the other hand, has an amplitude that is on par with the field-driven RAHE. So, it seems like the current switches the CoTb almost entirely. Half of the greatest resistance change occurs at a critical switching current (jc), which is equal to the jCoTb number. taken from Fig. According to 3b, the jc of this 6 nm thick sample was estimated to be around 9×10^4 A/m². Supplementary Note S2 presents the results of an investigation on how Hex affects jc.

Supplementary Note S8 compares the SOT switching efficiency of these CoTb gradient samples to that of (i) ferrimagnetic CoTb film SOT switching (with a bias magnetic field present) and (ii) field-free deterministic SOT switching of perpendicular ferromagnetic layers. The SOT switching efficiency is given by jc/(t exp(Keff)), where t is the thickness of the magnetic film and Keff is its effective perpendicular anisotropy energy density. Under all conditions, the CoTb samples with the vertical makeup gradient exhibited the best SOT switching efficiency.

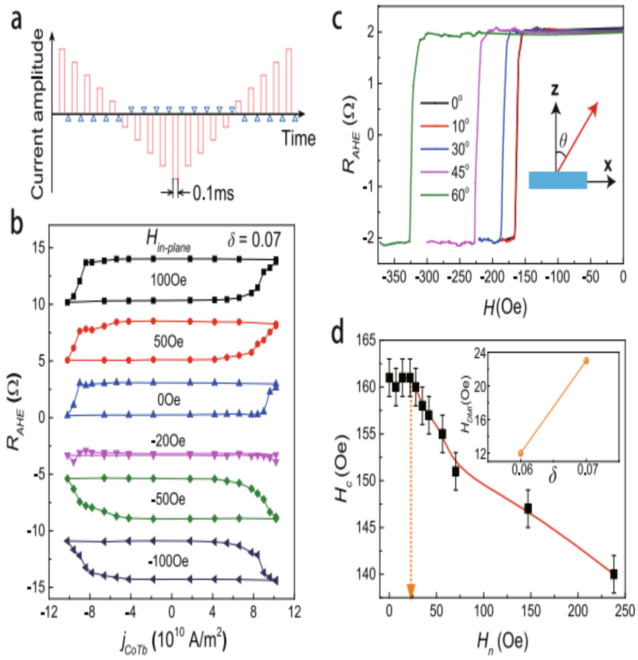

Figure. The DMI was measured after three attempts at SOT switching. for measuring the evolution of SOT. Potentially usable for writing purposes are pulses with a width of 0.1 ms that alternate between positive and negative states. In order to find out the magnetic state of the CoTb layer, AHE applied a read current that lasted one minute after each writing pulse. This section displays examples of Sample b SOT switching curves with different in-plane magnetic fields, such as zero-field and ε = 0.07. As the film's magnetization changes from up to down at different magnetic field angles compared to the film's typical direction, C AHE forms. What this means on the x-z plane is shown in the picture below. regarding Hn, how Hc feels. As soon as Hc goes beyond a certain point, it starts to drop. Obtaining error bars requires multiple measurements of each item. The picture in the insert shows how the link between δ and HDMI gets stronger when using 6 nm CoTb films.

When the Oe is equal to or less than 100, the switching circuits should have opposing switching polarities according to the SOT design. Plus, it's even more interesting that a whole SOT swapping cycle has been seen without Hex. Similar to the positive Hex examples, this field-free toggling loop has the same polarity. You can see almost every switching signal in this sample with Hex = -20 Oe. The presence of an effective internal field carrying out SOT flipping is proven by these findings. We postulate that the g-DMI of the CoTb layer is responsible for this beneficial field.

The magnetic droplet nucleation model36,51 served as the basis for our method of determining the g-DMI-induced effective field HDMI in our sample. similar to the one in Figure. Put in. To find the hysteresis loop's size, the magnetic field was angled with respect to the z-axis (see to 3c). In Figure 3c, we can see the magnetization flipping curves at different angles in the negative field range. To express the coercive field Hc and the corresponding in-plane field Hn, flip the magnetization from "up" to "down" and write Hswcos and Hswsin, respectively.

As seen in Figure 3d, the measured Hc is plotted against Hn. Like I said before, there's a clear plateau in the curve, and when Hn hits a certain amount, Hc starts to drop. At this level Hn, HDMI36,51 is equivalent. As a result, the 6 nm CoTb layer's HDMI was found to be approximately 23 Oe with ε = 0.07. We can see that this number is quite close to the value of the applied in-plane Hex (−20 Oe, see Fig. 3b), which is the point at which magnetization switching stops happening. This fits well with the theory that the field-free switching seen is caused by the g-DMI-induced effective field33–35. The following samples were subjected to SOT switching tests in order to gain a better comprehension of how the composition gradient affects the switching behavior: (A) 6 nm thick CoTb with δ = 0.06 per 1 nm; (B) 9 nm thick CoTb with δ = 0.07 per 1.5 nm; and (C) 4.2 nm thick CoTb with δ = 0.07 per 0.7 nm. Now, the composition gradient slope is not as steep as it was in the prior samples, which contained a 6 nm thick CoTb film with ε = 0.07 every 1 nm. Samples A and B exhibited noticeably thicker total CoTb layers and lower δ values, which is the rationale behind this. The composition gradient slopes upward higher in Sample C because its total CoTb thickness is lower for the same amount of ε.

Notes S3, S4, and S5 provide the results. Without Hex, each sample showed clear, predictable switching patterns. The HDMI measurement and the Hex number at which switching stopped were in good agreement. This agrees with the theory that the g-DMI was responsible for the inplane symmetry loss and zero field flipping observed in these samples. As anticipated, samples A and B exhibited higher jc values (>10 × 1010 A/m2) compared to the CoTb layer, which had a 6 nm thickness and a δ of 0.07. Sample C, on the other hand, showed a smaller jc (about 7.5 × 1010 A/m2) and a bigger HDMI (approximately 40 Oe), which was expected considering its steeper composition gradient. For field-free SOT switching, we also looked at how applied current history, device orientation, and wafer location affected the process. Further details regarding these studies can be found in Supplementary Notes S9 and S10. They prove that conventional lateral asymmetry does not impact switching by showing that the field-free switching polarity is unaffected by device orientation. Additionally, we found that the training effect of the applied writing current history controls the polarity of the succeeding current-induced switching loops. When numerous devices were tested on a 100 mm chip in different places, this pattern was constantly observed.

a

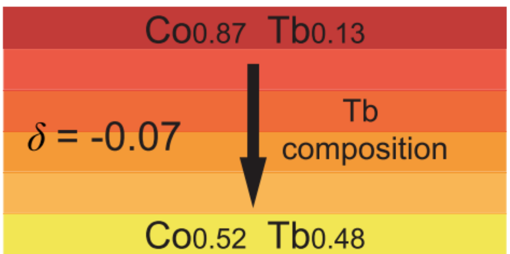

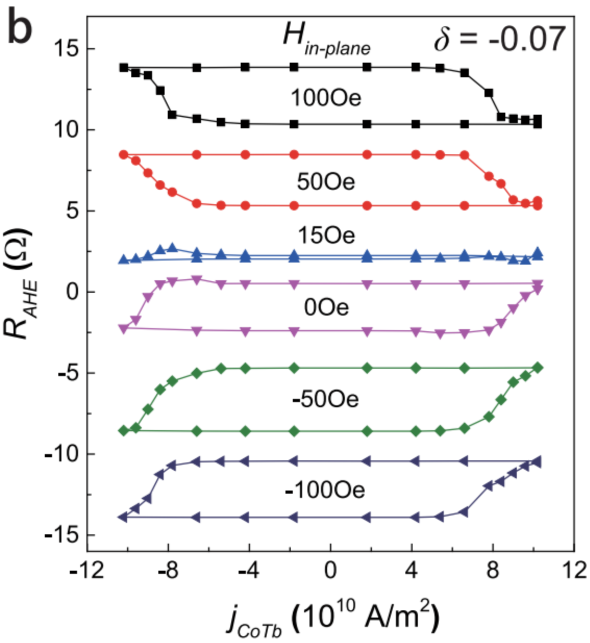

The process by which a CoTb film with a reversed composition gradient turns on and off. We investigated the on/off switching of SOTs and g-DMI in a 6 nm thick CoTb layer with an inverse composition gradient (ε = -0.07), where the Tb concentration dropped from the bottom to the top of the layers, to gain a better understanding of their origin. The SOT switching curves found for this sample under different hexadecimals are shown in Figure 4b, and other information about this sample is given in Figure 4a. The contrasting orientation of the switching loops with the sample with ε = 0.07 is continuously evident when comparing Figs. 4b and 3b.

This points to the fact that the two samples' vertical broken symmetry orientations are extremely dissimilar. This provides support for the idea that the vertical composition gradient is the source of the SOTs in the CoTb layer. In this case, we also saw SOT switching since the zero-field loop takes on the same orientation as switching loops when Hex is negative. A positive Hex value, or about 15 Oe, also stops the deterministic switching. Our fieldfree switching hypothesis asserts that g-DMI dictates both of these characteristics, which goes against our observations in the sample with ε = 0.07.

We can therefore assume that, like in the prior case, the inverse composition gradient also produces an HDMI of the opposite sign. The field-free switching data in Figure 4b can be explained by combining the fact that the SOT sign is backwards and the HDMI sign is forwards for our reference device. Figure 3b shows that this agrees with the predictions and calculations made by the models. To learn how this field-free switching works at its core, we used micromagnetic models. Our micromagnetism model is based on a two-sublattice model with a high exchange interaction. There is more than just the trading relationship that we think about. Our investigation also delves into the torque exerted by the anisotropy, DMI, and SOT. Other information A comprehensive explanation of the micromagnetic model is given in Note S6. From a modeling standpoint, the symmetry breaking is similar to the interfacial DMI seen in other layered systems, where the g-DMI is reliant on the composition gradient down the z-axis36.

To replicate the experimental setup, we begin by examining a cross shape that is completely saturated along the +z axis (see Fig. 2a). From this starting point, apply an electric current for 20 nanoseconds (from ton,1 to toff,1). After another 12 nanoseconds of rest, switch the current polarization from ton,2 to toff,2 and repeat the operation. The two current spikes and the average z component of the magnetization for the first sublattice over time are shown in Figure 5b (black line). The deterministic switching starts with the development of a domain at the edge of the sample, according to earlier numerical studies (see Fig. 5a), since the magnetization tends to an in-plane orientation controlled by the DMI boundary conditions.

Put simply, the application of the SOT to this in-plane component at the edge results in the creation of a new domain (Fig. 5c-e). A highly asymmetrical pattern of magnetization is generated by the combination of the DMI, exchange fields, and boundary conditions to enable switching. To see this in action, look at Figure 5f–h, where the DW velocity is higher around the edges than in the center. By the time the current stops flowing, the magnetization has flipped polarity and is back to the uniform ground condition (Fig. 5i-j). Figure S7 in Supplementary Note S7 shows the identical processes for bursts of current with opposite polarity. To explore a more realistic memory device architecture, we also ran similar simulations with a pillar 400 nm in diameter (see to Fig. S8 in Supplementary Note S7). The fundamental conclusions about the switching process hold true when this pillar shape is considered.

3. DISCUSSION

Our work showcases the implementation of a field-free DMI-SOT switching mechanism in a thick, uniform layer of CoTb exhibiting a composition gradient that increases. Strong SOTs and g-DMI are both caused by the growth path's broken structure inversion symmetry. The possibility of field-free switching at extremely low current densities is brought about by this gradient-driven switching approach, which might be implemented on a very large wafer. The SOT switching efficiency is far higher than in earlier tests with ferromagnets and in earlier experiments with typical CoTb layers that did not have a composition gradient, both of which used field-assisted switching. Our structure's SOT could be further improved by reacting with the right heavy metal layer to generate more interfacial SOT, which comes from the bulk of the CoTb gradient film. Keep in mind that we are still able to choose a heavy metal layer for the SOT despite the fact that our structure's g-DMI is derived from the bulk composition gradient. Because of this, designers have more freedom to experiment with their creations.

As a last point, we want to stress that magnetic tunnel junctions made of FIMs 60–62 have shown high rates of tunneling magnetoresistance (TMR) before. Consequently, SOT memory devices capable of reading TMR data can make use of the CoTb gradient films discussed in this paper. Our results, which are relevant to ferrimagnets, build on the existing concept of perpendicular magnetization switching produced by SOT using both internal and exterior fields. Additionally, they make it easier to design fast SOT memory configurations.

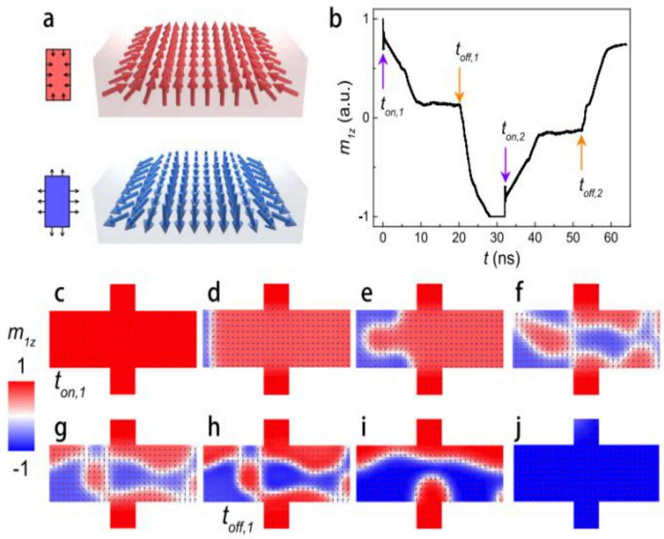

study of magnetic fields (Fig. 5). This demonstrates how the DMI border condition can induce magnetization tilting, which in turn allows domain nucleation at the edges. During the system transitions from 0 ns to 32 ns and 32 ns to 64 ns, we measure the average z component of the first sublattice magnetization with current flowing in opposite directions. Figures c-j show how the initial sublattice magnetization changes depending on the dynamics times (0-32 ns).

Methods

The sample's development and look. We used DC and RF sputtering to generate a series of Al (2)/CoTb (6)/Al (3) layers (thickness in nm) after heating and oxidizing silicon substrates at a pressure below 10−8 Torr. The deposition potential of the Co and Tb targets were adjusted to change the CoTb composition. The magnetic characteristics of each sample were examined using vibrating sample magnetometry. The JEMARM200F microscope was used to conduct the STEM and EDS examinations.

Device fabrication and electrical measurement.

The films were made on Hall bar devices with a 10 µm width using ion milling and optical lithography. The x-axis was used to apply DC current in order to quantify AHE and DMI. Current pulses with a width of 0.1 ms were used to perform the SOT switching tests. In order to assess the real intensities of the magnetic fields and ensure that there were no Hex contributions from residual fields, a Hall probe was inserted into the probe station. The first and second harmonic Hall voltages generated by an alternating current (AC) current with a frequency of 133.33 Hz were calculated using two SR830 lock-in amplifiers.

Data availability

In exchange for your convincing argument, the study's authors will gladly give you the data that backs up their conclusions.

REFERENCES

1. Shi, J. et al. Electrical manipulation of the magnetic order in anti ferromagnetic PtMn pillars. Nat. Electron. 3, 92–98 (2020).
2. Miron, I. M. et al. Perpendicular switching of a single ferromagnetic layer induced by in-plane current injection. Nature 476, 189–193 (2011).
3. Liu, L. et al. Spin–torque switching with the giant spin Hall effect of tantalum. Science 336, 555–558 (2012).
4. Emori, S., Bauer, U., Ahn, S. M., Martinez, E. & Beach, G. S. Current-driven dynamics of chiral ferromagnetic domain walls. Nat. Mater. 12, 611–616 (2013).
5. Cai, K. et al. Ultrafast and energy-efficient spin–orbit torque switching in compensated ferrimagnets. Nat. Electron. 3, 37–42 (2020).
6. Siddiqui, S. A. et al. Current-induced domain wall motion in a compensated ferrimagnet. Phys. Rev. Lett. 121, 057701 (2018).
7. Kim, K. et al. Fast domain wall motion in the vicinity of the angular momentum compensation temperature of ferrimagnets. Nat. Mater. 16, 1187–1192 (2017).
8. Han, J. et al. Room-temperature spin-orbit torque switching induced by a topological insulator. Phys. Rev. Lett. 119, 077702 (2017).
9. Zheng, Z. et al. Perpendicular magnetization switching by large spin orbit torques from sputtered Bi2Te3. Chin. Phys. B 29, 078505 (2020).
10. Cui, B. et al. Field-Free Spin-orbit torque switching of perpendicular magnetization by the Rashba interface. ACS Appl. Mater. Inter. 11, 39369–39375 (2019).
11. Oh, Y. W. et al. Field-free switching of perpendicular magnetization through spin-orbit torque in antiferromagnet/ferromagnet/oxide structures. Nat. Nanotechnol. 11, 878–884 (2016).
12. van den Brink, A. et al. Field-free magnetization reversal by spin-Hall effect and exchange bias. Nat. Commun. 7, 1–6 (2016).
13. Fukami, S., Zhang, C., Dutta Gupta, S., Kurenkov, A. & Ohno, H. Magnetization switching by spin–orbit torque in an antiferromagnet–ferromagnet bilayer system. Nat. Mater. 15, 535–541 (2016).
14. Lau, Y. C. et al. Spin–orbit torque switching without an external field using interlayer exchange coupling. Nat. Nanotechnol. 11, 758–762 (2016).
15. Liu, Y., Zhou, B. & Zhu, J. G. J. Field-free magnetization switching by utilizing the spin Hall effect and interlayer exchange coupling of iridium. Sci. Rep. 9, 1–7 (2019).
16. Zheng, Z. et al. Enhanced spin-orbit torque and multilevel current-induced switching in W/Co-Tb/Pt heterostructure. Phys. Rev. Appl. 12, 044032 (2019).